Kuhlmann, J.; Bartsch, I.; Willbold, E.; Schuchardt, S.; Holz, O.; Hort, N.; Hoeche, D.; Heineman, W.R.; Witte, F.:

Fast Escape of Hydrogen From Gas Cavities Around Corroding Magnesium Implants

In: Acta Biomaterialia (2012) Elsevier

DOI: 10.1016/j.actbio.2012.10.008

Fast Escape of Hydrogen From Gas Cavities Around Corroding Magnesium Implants

Julia Kuhlmann[1], Ivonne Bartsch[2,3], Elmar Willbold[2,3], Sven Schuchardt[4], Olaf Holz[4], Norbert Hort[5], Daniel Höche[5], William R. Heineman[1*], Frank Witte[2,3†]

[1] Department of Chemistry, University of Cincinnati, PO Box 210172, Cincinnati, OH 45221-0172, USA

[2] Laboratory for Biomechanics and Biomaterials, Orthopedic Clinic, Hannover Medical School, Anna-von-Borries-Str. 1-7, 30625 Hannover, Germany

[3] CrossBIT, Center for Biocompatibility and Implant-Immunology, Hannover Medical School, Feodor-Lynen-Str. 31, 30625 Hannover, Germany

[4] Fraunhofer Institute for Toxicology and Experimental Medicine (ITEM), Department for Bio- and Environmental Analytic, Nikolai-Fuchs-Str. 1, 30625 Hannover, Germany

[5] Helmholtz Zentrum Geesthacht, Max-Planck-Str. 1, 21502 Geesthacht, Germany

[*] Email: heinemwr@ucmail.uc.edu, Phone: +1-513-556-9210, Fax: +1-513-556-9239

[†] Email: witte.frank@mh-hannover.de, Phone: +49-511-532-8961, Fax: +49-511-532-8975

Abstract

Magnesium materials are of increasing interest in the development of biodegradable implants as they exhibit properties that make them promising candidates. However, formation of gas cavities after implantation of magnesium alloys is widely reported in literature. The gas composition and the concentration of in these bubbles are not clearly known as only a few studies using techniques not specific for were done about 60 years ago. Currently, many researchers assume that these cavities contain primarily hydrogen because it is a product of magnesium dissolution in aqueous media. In order to clearly answer this question, we implanted rare earth containing magnesium alloy disks in mice and determined the concentration of hydrogen gas for up to ten days using an amperometric hydrogen sensor and mass spectrometric measurements. We were able to directly monitor the hydrogen concentration over a period of ten days and to show that the gas cavities only contained a low concentration of hydrogen gas, even shortly after the formation of the cavities. This means that hydrogen must be exchanged very quickly after implantation. To confirm these results, hydrogen gas was directly injected subcutaneously and most of the hydrogen gas was found to exchange within the first hour after injection. Overall, our results disprove the common misbelief that these cavities mainly contain hydrogen and show how quickly this gas is exchanged with the surrounding tissue.

Keywords

Magnesium alloys, hydrogen, biodegradable implants, gas cavities, amperometric hydrogen sensor

1. Introduction

Metals have been used as internal fixtures to aid healing of fractured bones and tissue for more than 100 years [1]. Today, commonly used metals for these types of implants are stainless steel, Ti and Co-Cr alloys [2]. While these permanent implants are invaluable and generally biocompatible, they can cause problems such as stress shielding and the release of toxic metal ions through corrosion over time [1, 3]. Therefore, research groups are developing biodegradable (temporary) metallic implants, many of them focusing on Mg-based materials. Although Mg materials have traditionally been used for structural applications in the automotive and aerospace industry, they have gained attention in the orthopedic and biomedical engineering field [4, 5]. Their unique properties, which include physical and mechanical properties close to bone, make them promising candidates for biodegradable implants. Furthermore, these materials are generally non-toxic, lightweight and corrode rapidly in aqueous environments [6, 7]. During corrosion Mg is oxidized to Mg^{2+} as water is reduced to H_2 and OH^-. While the human body buffering system can compensate for the release of OH^- and some increase in Mg^{2+} is non-toxic [8], little is known about the fate of H_2 *in vivo*. The evolution of H_2 gas bubbles after adding Mg alloys to aqueous solutions has been observed extensively [9, 10] as well as the formations of gas cavities *in vivo* [11-13]. Two studies conducted over 60 years ago used techniques available at that time to analyze the gas composition of these cavities. E. D. McBride [14] reported in 1938 that gas samples aspirated from a cavity 40 d after implanting a band of Mg alloy, showed a gas composition of 5.6% CO_2, 6.5% O_2, 7.3% H_2 and 80.6% N_2. However, he did not state how the gas composition was

analyzed. In 1942, C. P. McCord *et al.* [15] used an interferometer to analyze the composition of gas samples drawn from gas gangrene formed in rats 5 d after Mg powder implantation. Their results showed a gas composition of 1.3% CO_2 and 15.2% O_2, and they calculated that the H_2 concentration must have been 2.2% using a method described by J. D. Edwards [16]. Additionally, their efforts to ignite the gas sample failed, which led to the conclusion that the sample must have contained less than the 4.1% H_2 required for ignition in air. More recently, Witte *et al.* [17] also tried to ignite samples withdrawn from gas cavities, but no combustion was observed. While these studies suggested that H_2 might not be the major component in these gas cavities, they did not directly measure H_2 nor did they use current analytical methods to determine the concentration of H_2. More importantly, while these studies remain the only ones attempting to analyze the H_2 concentration, it is often still assumed that gas cavities formed during Mg material corrosion *in vivo* contain primarily H_2 [18-21]. Nevertheless, highly selective analytical techniques to measure H_2 are available. An electrochemical sensor for H_2, analogous to the commonly used Clark O_2 sensor, has previously been used *in vivo* to determine local blood flow with the H_2 washout technique [22]. This amperometric sensor detects H_2 by selectively oxidizing H_2 to H^+. Although this sensor is not implantable, it would enable measurement on surface of the gas cavities. Mass spectrometry is another commonly used analytical technique that would allow direct analysis of H_2 and any other gases in the cavity.

Here we report a method to directly analyze the H_2 concentration and the gas composition of gas cavities formed during *in vivo* degradation of subcutaneously

implanted rare-earth containing Mg alloys disks. We used an amperometric H_2 sensor and mass spectrometry to analyze the gas in the cavities over the course of 10 d thereby providing a time course for H_2 behavior *in vivo*. After the experiment, we analyzed the response of the skin covering the alloy disks and corrosion behavior of the alloys. Our results are especially significant in that they alleviate concerns about H_2 gas accumulating in the bodies of implant patients.

2. Method and Materials

2.1 Mg alloy preparation

The Mg alloy MgY4wt%Gd0.5wt%Nd2wt%Dy0.5wt% has been prepared using pure elements by direct chill permanent mold casting according to standard procedure as describe by Elsayed *et al.* [23]. All casting operations were performed under a protective gas (Ar-2% SF6). Pure Mg was molten under protective gas in a mild steel crucible. At a melting temperature of 730 °C the alloying elements Y, Nd, Gd and Dy have been added. The alloy was stirred for 20 min with 150 rpm. Afterwards the melt was poured into a thin walled (3 mm thickness) mold made of mild steel. The mold was then kept in a holding furnace at 680 °C for 1 h to homogenize the melt. After holding, the mold was dipped into flowing water (15 °C) to solidify the material and to produce a casting. The Mg alloy disks (8.0 mm diameter, 1.5 mm thickness) were machined from cast material, polished by SiC emory paper (up to 4000), briefly etched and cleaned in 100% ethanol in

an ultrasonic bath. All disks were gamma-sterilized by 27 kGy of ^{60}Co radiation and had an average weight of 141.2 ± 1.3 mg before implantation.

2.2 Animal model

The animal experiment was conducted under an ethic committee approved protocol in accordance with German federal animal welfare legislation (Ref.-No. 33.9-42502-04-08/1499) and in accordance with the National Institute of Health guidelines for the use of laboratory animals. Ten female hairless mice from the Charles River Laboratories (Crl: SKH1-*hr*) aged from 12 to 24 weeks were used in this study. These mice are hairless but immunocompetent. Their fur is normal up to 10 d, and then the hair is gradually lost, starting around the nose. Around day 20 the fur is lost completely. The average weight of the used mice was about 26 g. After the implantation each mouse was housed individually and was fed a standard diet (altromin1324) and water *ad libitum*. Rooms of animal husbandry were illuminated by artificial light 14 h a day starting at 7 a.m.. The mice were anaesthetized by intraperitoneal injection of 2% xylazine (10 mg/kg body weight; Rompun®, Bayer Health Care, Leverkusen, Germany) and 10% ketamine (100 mg/kg body weight; KetaminGräub®, Albrecht GmbH, Aulendorf, Germany). In order to avoid cooling of the body, mice were placed on a custom-made heating plate during surgery and measurements. Dorsal skin was cleaned according to chirurgical guidelines. Two longitudinal incisions (one in the shoulder region, one in the lumbar region) of 1.0 cm each were made in the median line through the full thickness of the skin. Subcutaneous pockets between the fascia of the dorsal muscles and the subcutaneous

tissue were created by blunt dissection with scissors. The implants were placed in these pockets. The Mg implants were placed in the shoulder and lumbar region. The skin was closed with resorbable surgical suture material (Vicryl, Ethicon, Johnson & Johnson GmbH, Germany).

For the H_2 injection experiments, H_2 (99.999%) was injected subcutaneously in hairless mice (three mice per time point). The gas was withdrawn with gastight syringes 1, 2, 4 and 12 h after injection and analyzed with mass spectrometry as described in subsection 2.3.

2.3 H_2 measurements

Amperometric H_2 measurements were performed using a H_2 microsensor (50 µm tip diameter) connected to a multimeter (both from Unisense, Aarhus, Denmark) that was polarized at +800 mV for at least 1 h [24]. After a stable current in the low picoampere range was established, the amperometric sensor was ready to be used. The sensor was calibrated by adding known amounts of H_2 saturated deionized H_2O to a known volume of deionized H_2O (according to manufacturer recommendations [24, 25]). Measurements were taken for three minutes on the skin on top of the gas cavities and subcutaneously in an incision on top of the gas cavities. As a control, measurements were taken on top of the skin in an area without any gas cavities. Standard deviation (error bars on graph) were calculated from the averaged first 100 data points taken during each of the 3 min measurements. Microsensor readings were converted into % v/v for comparison with

mass spectrometry data. The manufacturer reported the limit of detection to be 0.02% (0.1 μM) in H_2O.

For mass spectrometry the gas samples were withdrawn from the cavities using 2.5-mL gastight syringes (Hamilton Messtechnik GmbH, Höchst, Germany). The needles were covered with a septum until the samples were analyzed with the SMart Nose® volatile organic compound analyzer system (former Smartnose SA, Switzerland), which was fitted with a special injection device and a capillary for gas phase transfer purposes. The analysis was performed with gas samples as received without any further preparation. About 1 to 2 mL of each sample were introduced to the injection port heated at 22 °C. Before injection the N_2 flow was stopped for 20 s and the acquisition was started simultaneously with the opening of the gas outlet. Data was acquired at 70 eV, from 1 to 60 m/z, conducting four cycles within 150 s. The averaged cycles 2 to 4 were used for data analysis. After each injection the entire system was purged with N_2 at a flow rate of 80 mL/min for two minutes. The system was calibrated with pure gas samples of H_2 (99.999%), O_2 (99.5%), and CO_2 (99.995%) as well by gas mixtures of H_2 and CO_2 injected in amount from 0.1 to 1.0 mL under similar conditions.

2.4 Histology

The excised tissue samples were fixed in 3.7% commercial formalin (Otto Fischer, Saarbrücken, Germany), embedded and sectioned in paraffin. Then they were stained with Mayer's hematoxylin (Merck KGaA, Darmstadt, Germany) and 1% eosin (Merck KGaA, Darmstadt, Germany) and mounted in Eukitt (Labonord, Mönchengladbach,

Germany) according to standard procedures. We performed at least five histomorphometric measurements per H&E cross-section of each mouse biopsy and analyzed ten skin biopsies from 2-day and 10-day mice as well as four full skin biopsies of the controls.

2.5 XPS Material analysis and corrosion rate determination

X-ray induced photoelectron spectroscopy (XPS) experiments were done on a KRATOS AXIS Ultra DLD system (Manchester, UK) equipped with a 15 kV X-ray gun using monochromatic Al K_α radiation. The analyzed area size was 700 x 300 µm positioned in the center of the sputter area (2 x 2 mm). Energy resolution was set to a pass energy of 20 eV for high-resolution region measurements. A charge neutralizer was applied to correct for the chemical shifts caused by the nonconductive corrosion products. For depth profiling Ar ions (Ar^+ at 4 keV) were used to etch the samples. The applied sputter rate was approximately 25 nm/min. The following core levels were analyzed: Mg 2*p*, O 1*s*, C 1*s*, N 1*s*, Na 1*s*, Ca 2*p*, P 2*p*, Gd 3*d*, Y 3*d*, Nd 3*d* and Dy 4*p* to determine the depth distribution. Curve fitting and deconvolution of the O 1*s* spectra was performed with CasaXPS 2.315 software (Casa Software Ltd., UK). The binding energy can be estimated to an accuracy of ±0.3 eV. The corrosion layer thickness was measured on micrographs of metallographic specimen of the corroded Mg samples after 2 d and 10 d of subcutaneous implantation using ImageJ software.

The corrosion rate was determined after the explanted Mg alloy disks were treated with 180 g/L CrO_3 to remove the corrosion products at 22 ˚C for 20 min. Difference in

weight before and after implantation was used to calculate the corrosion rate in mm/year as described elsewhere [26].

3. Results and Discussion

We implanted fast corroding rare-earth element containing Mg alloy disks (8.0 x 1.5 mm, permanent mold cast, machined + polished, Mg4Y2Nd0.5Gd0.5Dy) with an average weight of 141.2 ± 1.3 mg subcutaneously in ten hairless mice (Crl: SKH1-*hr*) for up to 10 d. We chose this alloy since it corrodes fast and has previously been shown to produce large gas cavities *in vivo*. Two Mg alloy disks (one for each type of measurement) per mouse were placed subcutaneously under sterile conditions. H_2 evolution was monitored over 2 d (2-day group) and 10 d (10-day group) with five mice per group. The mice started showing clinically visible subcutaneous gas cavities about 24 h after implantation (Fig. 1) and the visible size of these cavities increased during the course of the experiment.

A H_2 microsensor from Unisense with a 50 μm tip diameter, calibrated following the manufacturer's recommendations was used for the amperometric measurements. The mice were anesthetized and a 1 cm long incisions close to the gas cavities around the disk implanted in the left shoulder region were made using a sterile surgical scalpel. The anesthetized mice were immobilized on a heated swiveling table and the microsensor was positioned with a micromanipulator (Fig. 2). Measurements were taken on the skin on top of the gas cavities, in the incision on top of the fibrous tissue layer engulfing the gas

cavities and on the skin in a control area. We were able to measure H_2 on the skin on top of the gas cavities. This indicated that the H_2 at least partially exchanges through the skin, which could be facilitated by enrichment of H_2 in the fatty tissue or oily layer of the skin, as H_2 is more soluble in oils than in aqueous solutions. However, the results from these measurements were generally slightly lower compared to measurements in the incision. Measurements inside the gas cavities were done in preliminary experiments by piercing the tissue engulfing the gas cavities with the microsensor (data not shown). These experiments showed that there was no significant difference between measuring inside the cavity as compared to measuring on the top of the tissue engulfing the cavity. Since it was not always possible to pierce the tissue with the microsensor and there was not significant difference between the measurements, we decided to only measure in the incisions on top of the tissue. The H_2 concentration in the incisions ranged from 97 ± 46 µM (0.2 ± 0.1% v/v) to 305 ± 32 µM (0.69 ± 0.07% v/v) 1 d after surgery and from 95 ± 34 µM (0.22 ± 0.08% v/v) to 428 ± 35 µM (0.97 ± 0.08% v/v) 2 d after surgery for the 2-day group (Fig. 3a). On average, a minimal increase in H_2 over the course of 2 d was observed. For the 10-day group (Fig. 3b), the results varied considerably among mice. After 2 d the H_2 concentration in the incisions ranged from 66 ± 32 µM (0.15 ± 0.07% v/v) to 611 ± 44 µM (1.4 ± 0.1% v/v) and from 258 ± 36 µM (0.59 ± 0.08% v/v) to 391 ± 31 µM (0.89 ± 0.07% v/v) after 5 d. The experiment was completed ten days post surgery due to animal welfare associated with the very large size of the gas cavities. At that point (Fig. 3b) the H_2 concentration in the incision ranged from 361 ± 91 µM (0.8 ± 0.2% v/v) to 507 ± 38 µM (1.15 ± 0.09% v/v) with two data points above the upper limits of the

calibration curve (>805 μM (>1.8% v/v), data points not included on graph). The variation in the 10-day group is due to the free-moving Mg disk inside the gas cavity. During the free-disk-movement the protective corrosion layer is destroyed and thus Mg corrosion is forced depending on the mouse activity level.

We used mass spectrometry (MS) to confirm the results from the amperometric microsensor and to analyze the composition of the gas. Gas samples were withdrawn from the cavities in the right lumbar region with a gas-tight syringe and injected into a volatile organic compound analyzer system (Smart Nose®). The H_2 concentration was between 0.05 ± 0.04% v/v and 0.12 ± 0.04% v/v two days after surgery (Fig. 4a) and the CO_2 concentration was between 0.15 ± 0.04 and 0.18 ± 0.04% v/v. Ten days after surgery (Fig. 4b), the H_2 concentration ranged from 0.06 ± 0.04% v/v to 0.30 ± 0.04% v/v and the CO_2 concentration was between 0.08 ± 0.04% v/v and 0.12 ± 0.04% v/v. These results confirmed the amperometric measurements. Additionally, there was no significant difference in O_2 and N_2 concentration and no other gases were detected.

To analyze how quickly H_2 exchanges, we injected H_2 subcutaneously in hairless mice (three mice per time point). After 1, 2, 4 and 12 h the gas was withdrawn and analyzed with the Smart Nose® system (Fig. 5). The H_2 concentration dramatically decreased to as low as 0.22 ± 0.04% v/v after only 1 h and was almost completely exchanged (0.02 ± 0.04% v/v) after 12 h. This indicates that the exchange of H_2 occured very rapidly, while the gas cavity did not significantly change in size.

Tissue samples were taken from the skin covering the implants for histological analysis to gain insight into the gas exchange process. The hematoxylin and eosin (H&E)

stained histology showed a slightly thicker fibrous capsule (204 ± 18 μm) around the gas cavity after 2 d (Fig. 6a), which decreased in thickness to 120 ± 17 μm after 10 d (Fig. 6b). This is in the normal range of physiological mouse fascia (157 ± 23 μm), as shown in control samples (Fig. 6c) taken from the same mouse. One could argue that the thicker fibrous capsule after 48 h (Fig. 6a) could have kept more H_2 inside the cavity, since the diffusion distance through the skin is greater than after 10 d (Fig. 6b). However, the H_2 concentration was lower at 2 d than after 10 d. On the other hand, the thicker tissue layer would allow more H_2 to saturate in the surrounding tissue thus leading to a lower concentration of H_2 in the cavity. This could mean that the gas exchange through the skin is not the major path of exchange. Additionally, the difference in size of the vacuoles seen in the skin sections of the test and control samples are a normal observation in this type of mouse model as described elsewhere [27].

To better understand this result, we analyzed the corroded Mg disks with X-ray induced photoelectron spectroscopy (XPS) and determined the corrosion rate from the weight loss of the explanted Mg alloy disks after removing the corrosion products with chromic acid as described elsewhere [26]. The XPS analysis revealed that the bulk matrix primarily determines the corrosion properties of the alloy, while intermetallics like $Mg_{41}Nd_5$ or $Mg_{24}Y_5$ (Fig. 7) revealed in slightly modified degradation properties as described by M. Liu *et al.* [28]. The results of the XPS measurements (Fig. 8) are for two disks implanted at the lumbar region for 2 d and 10 d, respectively. To analyze the corrosion products the composition of body fluids that were in contact with the material and the most common inorganic compounds (PO_4^{3-}, CO_3^{2-} and Ca compounds) beside

water [29] needed to be considered. The determined elemental distribution represented only the outer 5 µm of the corrosion layer, not the elemental distribution through the whole thickness of the corrosion layer. The sample from the 2-day group (Fig. 8a) had a 1-µm thick corrosion active dissolution interaction zone consisting of $Mg(OH)_2$. The high-resolution scan of the O 1*s* state shows the different excitation states. Below the dissolution region, different amounts of CO_3^{2-}, O^{2-}, PO_4^{3-} and other high order compositions (Fig. 8, marked by X) were found. These results were comparable to Abidin's work [30]. The shift of electrochemical potential and corrosion currents depends on the amount of intermetallic phases, while the quantity of reacting rare earth elements depends on their reactivity [31]. Y_2O_3 and $Y(OH)_3$ for example has been formed comparable to the $Mg(OH)_2$ zone among Mg-O-X compounds. Other probable compounds are hydroxyl apatites based on Ca or P in aqueous bonding as well as rare-earth compounds like $NdPO_4$ [32]. The substantial increase in thickness of the corroded layer after ten days is displayed in the depth profile (Fig. 8b). Organic compounds (e.g. from proteins) interacting at the disks can account for the large concentration of carbon atoms. The O 1*s* level showed a OH^- zone down to approximately 5 µm. For longer duration *in vivo* the influence of rare-earth elements slows down, acting as *degradation brakes* as explained by Yao in case of Y [33]. Shortly after implantation strong H_2 evolution occurs and then the degradation rate stabilizes. Due to the environmental interaction and passivation, stable compounds were formed, which enhanced the growth of the corrosion layer. Finally, a very inhomogeneous surface structure arises and this mixture of organics, CO_3^{2-} and OH^- determines the disk degradation properties. It seems

that the elemental composition of the outer corrosion layer changed during the time course of the 10 d implantation. The analysis of the corrosion layer thickness performed after the XPS analysis revealed that the thickness increased from 27.5 ± 10.5 µm after 2 d to 201 ± 107 µm after 10 d. Overall, this supports the findings of the corrosion rate determination from weight loss, which revealed that the 10-day implants corroded faster (20.7 ± 13.1 mm/year) than the 2-day implants (8.6 ± 9.9 mm/year).

Based on the results of our study, the known physical properties of H_2 and the low concentration of H_2 in the atmosphere and the body [34], we propose the following potential exchange mechanism in which the concentration gradient between the gases in the initially formed gas cavity, the adjacent tissue and the atmosphere seems to be the main driving force behind the exchange. The corrosion of the alloy disks starts immediately after implantation and the initial evolution of H_2 drives the formation of the cavity, pushing surrounding tissues layers apart. Simultaneously, H_2 is expected to saturate the adjacent tissues although the solubility of H_2 in cells and aqueous media such as biological fluids is low [35, 36]. While the alloy disks continue to corrode and the size of the cavities increases, the evolving H_2 in the growing cavities continuously exchanges with dissolved gases like N_2, O_2 and CO_2 from the neighboring tissues and blood vessels [37]. Diffusion of H_2 through the skin is occurring as well, since we were able to measure H_2 on top of the skin at about the same level as directly on the bubble. However, this type of exchange may be too slow to be the main path of exchange. As the corrosion behavior of the alloy changes over the course of 10 d, the size of the gas cavities as well as the H_2 concentration in the cavities increased. This can be explained by an increased corrosion

rate that must be slightly higher than the exchange rate of H_2. Previous studies also reported that the cavities disappear several months after implantation [20], which means that the corrosion rate of the implant material and thus the evolution rate of H_2 falls below the exchange rate of H_2.

4. Conclusion

In this study we were able to directly measure the concentration of H_2 in subcutaneous gas cavities with an amperometric H_2 microsensor over the course of ten days. The results were confirmed by mass spectrometry, which was also used to determine the gas composition. The results show that the observed subcutaneous gas cavities only contained a low concentration of H_2 even shortly after implantation, which leads to the conclusion that H_2 is readily exchanged *in vivo*. Furthermore, we injected H_2 subcutaneously to determine how quickly it is exchanged. With these experiments we were able to show that H_2 is exchanged very quickly after implantation as there was only a very low concentration detected 1 d after surgery and within an hour after subcutaneous injection of H_2. We also detected H_2 on top of the skin, which suggests that H_2 readily exchanges through the skin and/or accumulates in fatty tissue, as it is more soluble in non-polar solvents as compared to body fluids. During 10 d, the size of the cavities as well as the H_2 concentration increased. The increase in corrosion rate and corrosion layer after 10 d could explain the increase in size of the gas cavity as well as the slight increase in H_2 concentration, given that H_2 exchanges at a constant rate. Although the exact nature

of this exchange and the formation of the cavities are not clear, diffusion through the skin as well as diffusion into capillaries and transport by the vascular system might be essential as outlined in the proposed exchange mechanism. These findings apply to subcutaneous gas cavities, but further research is needed to evaluate if the exchange behavior still applies when more tissues layers cover the cavities (as found after implantation in bone). Our conclusions support the hypothesis McBride and McCord drew over 60 years ago that H_2 absorbs as rapidly as it is formed when the oxidation of the metal is slow [14, 15] even though in their experiments H_2 was not directly measured and the measurements were done 40 d after implantation.

These results suggest that toxicity resulting from high concentrations of H_2 accumulating in tissue adjacent to an implant consisting of Mg or Mg alloy may not be an insurmountable problem in the practical application of these materials.

Acknowledgements

The authors thank Maria Brauneis and Maike Haupt at the CrossBIT, Sophie Müller, Heike Achilles and Mattias Reebmann at Laboratory for Biomechanics and Biomaterials at the Hannover Medical School (MHH) as well as Bianca Lavae-Mokhtari at the Fraunhofer Institute for Toxicology and Experimental Medicine (ITEM) in Hannover for their technical support. Additionally, the authors thank Gerald B. Kasting from the Department of Pharmaceutics & Cosmetic Science at the University of Cincinnati for helpful discussion about the gas exchange processes. The study was supported by the

NSF Engineering Research Center for Revolutionizing Metallic Biomaterials (NSF EEC 0812348).

References

[1] Uhthoff HK, Poitras P, Backman DS. Internal plate fixation of fractures: Short history and recent developments. Journal of Orthopaedic Science. 2006;11:118-26.
[2] Agrawal CM. Reconstructing the human body using biomaterials. Journal of the Minerals, Metals and Materials Society. 1998;50:31-5.
[3] Witte F, Hort N, Vogt C, Cohen S, Kainer KU, Willumeit R, et al. Degradable biomaterials based on magnesium corrosion. Current Opinion in Solid State and Materials Science. 2008;12:63-72.
[4] Staiger MP, Pietak AM, Huadmai J, Dias G. Magnesium and its alloys as orthopedic biomaterials: A review. Biomaterials. 2006;27:1728-34.
[5] Di Mario C, Griffiths H, Goktekin O, Peeters N, Verbist J, Bosiers M, et al. Drug-eluting bioabsorbable magnesium stent. Journal of Interventional Cardiology. 2004;17:391-5.
[6] Zeng R, Dietzel W, Witte F, Hort N, Blawert C. Progress and Challenge for Magnesium Alloys as Biomaterials. Advanced Engineering Materials. 2008;10:B3-B14.
[7] Song GL, Atrens A. Understanding Magnesium Corrosion: A Framework for Improved Alloy Performance. Advanced Engineering Materials. 2003;5:837-58.
[8] Saris N-EL, Mervaala E, Karppanen H, Khawaja JA, Lewenstam A. Magnesium. An update on physiological, clinical and analytical aspects. Clinica Chimica Acta. 2000;294:1-26.
[9] Song GL. Recent Progress in Corrosion and Protection of Magnesium Alloys. Advanced Engineering Materials. 2005;7:563-86.
[10] Song GL, Atrens A. Corrosion mechanisms of magnesium alloys. Advanced Engineering Materials. 1999;1:11-33.
[11] Witte F, Reifenrath J, Müller PP, Crostack HA, Nellesen J, Bach FW, et al. Cartilage repair on magnesium scaffolds used as a subchondral bone replacement. Materialwissenschaft und Werkstofftechnik. 2006;37:504-8.
[12] Kaya RA. The effects of magnesium particles in posterolateral spinal fusion an experimental in vivo study in a sheep model. Journal of Neurosurgery Spine. 2007;6:141-9.
[13] von der Höh N, Bormann D, Lucas A, Denkena B, Hackenbroich C, Meyer-Lindenberg A. Influence of Different Surface Machining Treatments of Magnesium-based Resorbable Implants on the Degradation Behavior in Rabbits. Advanced Engineering Materials. 2009;11:B47-B54.
[14] McBride ED. Absorbable Metal in Bone Surgery. Bone Surgery. 1938;111:2464.
[15] McCord CP, Prendergast JJ, Meek SF, Harrold GC. Chemical gas gangrene from metallic magnesium. Industrial Medicine. 1942;11:71-5.
[16] Edwards JD. Application of the Interferometer to Gas Analysis. Chemical and Metallurgical Engineering. 1919;21:560-5.
[17] Witte F, Kaese V, Haferkamp H, Switzer E, Meyer-Lindenberg A, Wirth CJ, et al. In vivo corrosion of four magnesium alloys and the associated bone response. Biomaterials. 2005;26:3557-63.
[18] Song GL. Control of biodegradation of biocompatable magnesium alloys. Corrosion Science. 2007;49:1696-701.
[19] Erdmann N, Bondarenko A, Hewicker-Trautwein M, Angrisani N, Reifenrath J, Lucas A, et al. Evaluation of the soft tissue biocompatibility of MgCa0.8 and surgical steel 316L in vivo: a comparative study in rabbits. Biomed Eng Online. 2010;9:63.
[20] Li Z, Gu X, Lou S, Zheng Y. The development of binary Mg-Ca alloys for use as biodegradable materials within bone. Biomaterials. 2008;29:1329-44.
[21] Zhang S, Zhang X, Zhao C, Li J, Song Y, Xie C, et al. Research on an Mg-Zn alloy as a degradable biomaterial. Acta Biomater. 2010;6:626-40.
[22] Pelzer M, Larsen M, Friedrich PF, Bishop AT. Measurement of bone blood flow using the hydrogen washout Technique-Part I: quantitative evaluation of tissue perfusion in the laboratory rat. J Orthop Res. 2008;26:741-5.

[23] Elsayed FR, Hort N, Salgado Ordorica MA, Kainer K. Magnesium Permanent Mold Castings Optimization. Materials Science Forum. 2011;690:65-8.
[24] Unisense AS. Hydrogen sensor user manual. In: A/S U, editor. Aarhus: Unisense A/S; 2010. p. 1-17.
[25] Wiesenburg DA, Guinasso NL. Equilibrium solubilities of methane, carbon monoxide, and hydrogen in water and sea water. Journal of Chemical and Engineering Data. 1979;24:356-60.
[26] Hort N, Huang Y, Fechner D, Stormer M, Blawert C, Witte F, et al. Magnesium alloys as implant materials--principles of property design for Mg-RE alloys. Acta Biomater. 2010;6:1714-25.
[27] Benavides F, Oberyszyn TM, VanBuskirk AM, Reeve VE, Kusewitt DF. The hairless mouse in skin research. J Dermatol Sci. 2009;53:10-8.
[28] Liu M, Schmutz P, Uggowitzer PJ, Song G, Atrens A. The influence of yttrium (Y) on the corrosion of Mg-Y binary alloys. Corrosion Science. 2010;52:3687-701.
[29] Green EL. Biology of the Laboratory Mouse; By the Staff of The Jackson Laboratory. Earl L. Green, Ed: McGraw-Hill; 1966.
[30] Zainal Abidin NI, Martin D, Atrens A. Corrosion of high purity Mg, AZ91, ZE41 and Mg2Zn0.2Mn in Hank's solution at room temperature. Corrosion Science. 2011;53:862-72.
[31] Bernal S, Blanco G, Gatica JM, Pérez-Omil JA, Pintado JM, Vidal H. Chemical Reactivity of Binary Rare Earth Oxides. In: Adachi G, Imanaka N, Kang ZC, editors. Binary Rare Earth Oxides: Springer Netherlands; 2005. p. 9-55.
[32] Poitrasson F, Oelkers E, Schott J, Montel J-M. Experimental determination of synthetic NdPO4 monazite end-member solubility in water from 21°C to 300°C: implications for rare earth element mobility in crustal fluids. Geochimica et Cosmochimica Acta. 2004;68:2207-21.
[33] Yao HB, Li Y, Wee ATS. Passivity behavior of melt-spun Mg-Y Alloys. Electrochimica Acta. 2003;48:4197-204.
[34] Holleman AF, Wiberg E. Lehrbuch der Anorganischen Chemie. 101. ed. Berlin New York: Walter de Gruyter & Co.; 1995.
[35] Power GG, Stegall H. Solubility of gases in human red blood cell ghosts. Journal of Applied Physiology. 1970;29:145-9.
[36] Van Slyke DD, Sendroy JJ. Studies of Gas and Electrolyte Equilibria in Blood. XI. The Solubility of Hydroge at 38˚ in Blood Serum and Cells. J Biol Chem. 1928;78:801-5.
[37] Kety SS. The theory and applications of the exchange of inert gas at the lungs and tissues. Pharmacological Reviews. 1951;3:1-41.

Figures

Fig. 1. A hairless but immunocompetent mouse is shown one day after the implantation of rare-earth element containing Mg alloy disks. Arrows indicate the development of clinically visible subcutaneous gas cavities around the implants.

Fig. 2. Experimental setup for amperometric measurements. An anesthetized mouse is positioned on a swiveling table, which is connected to a peristaltic pump and heated to 37 ˚C by a water bath. A H_2 microsensor is mounted in a micromanipulator and positioned in an incision in the skin of a hairless mouse to record a blank reading before implantation.

Fig. 3. Results of the amperometric H_2 sensor measurements for the (a) 2-day and the (b) 10-day group. Measurements were taken on the skin on top of the gas cavities (*skin*), in the incision on top of the gas cavities (*incision*) and on a control area (*control*). Results shown not blank corrected.

Fig. 4. Mass spectrometry. Results of the mass spectrometric gas analysis of samples withdrawn from cavities (a) 2 d and (b) 10 d after implantation.

Fig. 5. H_2 Injection. Results of the H_2 injection experiments with three mice per time point showed that the H_2 concentration 1 h after injection was below 0.6 ± 0.04% v/v. At the 12-hour time point, it further decreased below 0.2 ± 0.04% v/v. The CO_2 concentration stayed constant throughout the experiment.

Fig. 6. H&E stained histology of skin samples. Full skin cross-sections of mouse skin that covered the gas cavities (a) 2 d and (b) 10 d after surgery and (c) control sample are shown. (★) indicates fibrous capsule. (*) indicates physiological dermal cysts.

Fig. 7. The microstructure of a Mg alloy implant. Large grains and their growth directions are shown. Mg-rare earth intermetallics $Mg_{41}Nd_5$ or $Mg_{24}Y_5$ are visible at interdendritic regions. Mg rare earth phases and the bulk matrix are in competition regarding corrosion surface reactions.

Fig. 8. XPS analysis of corrosion layer on alloy disks. Elemental depth profiles of disks implanted at lumbar region for (a) 2 d and (b) 10 d are shown. Elemental depth profiles (top) and high-resolution scans at the O 1*s* state (bottom) give information about the distribution of different compounds (12000 s sputtering are approx. 5 µm).

Figure 1

Figure 2

Figure 3a

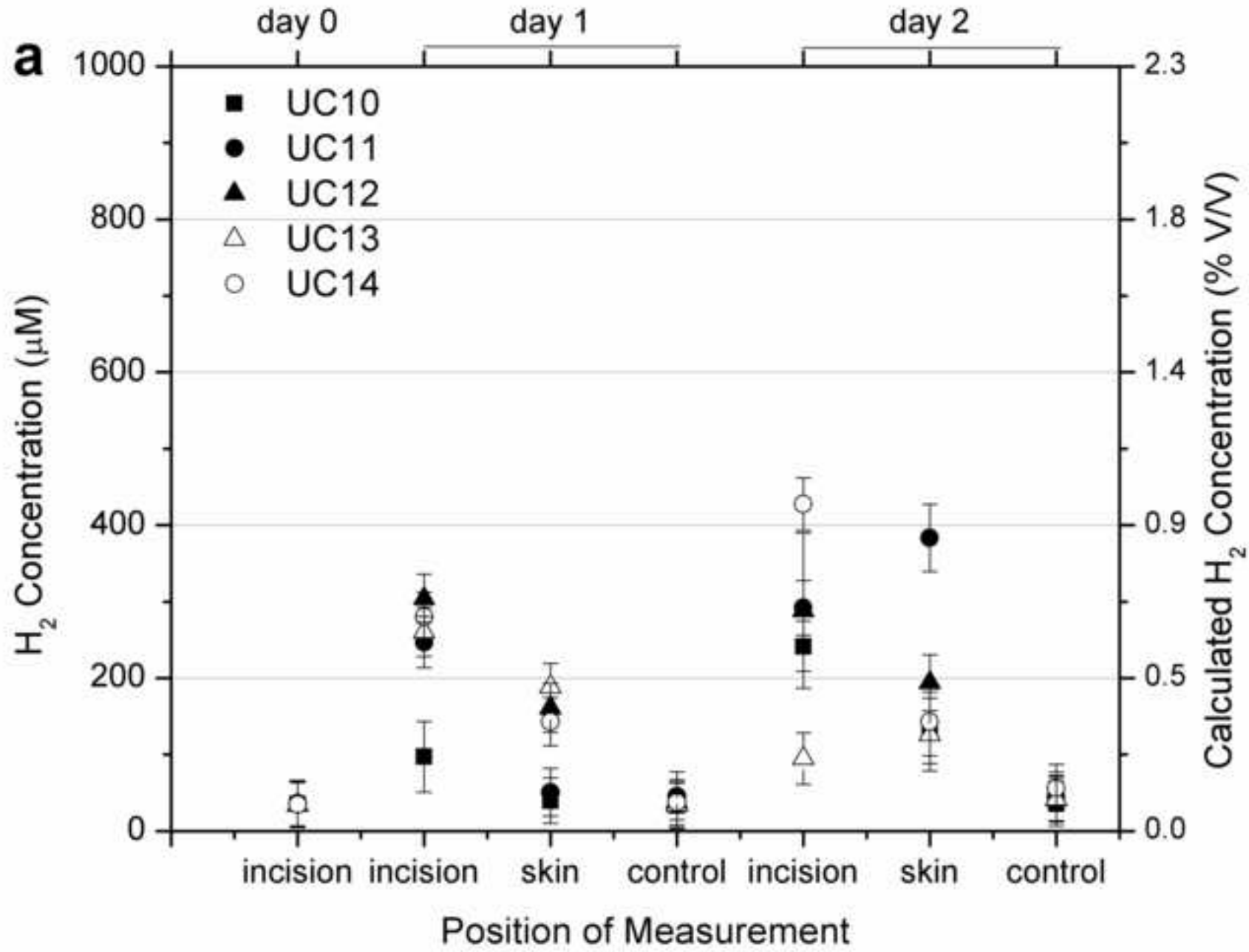

Figure 3b

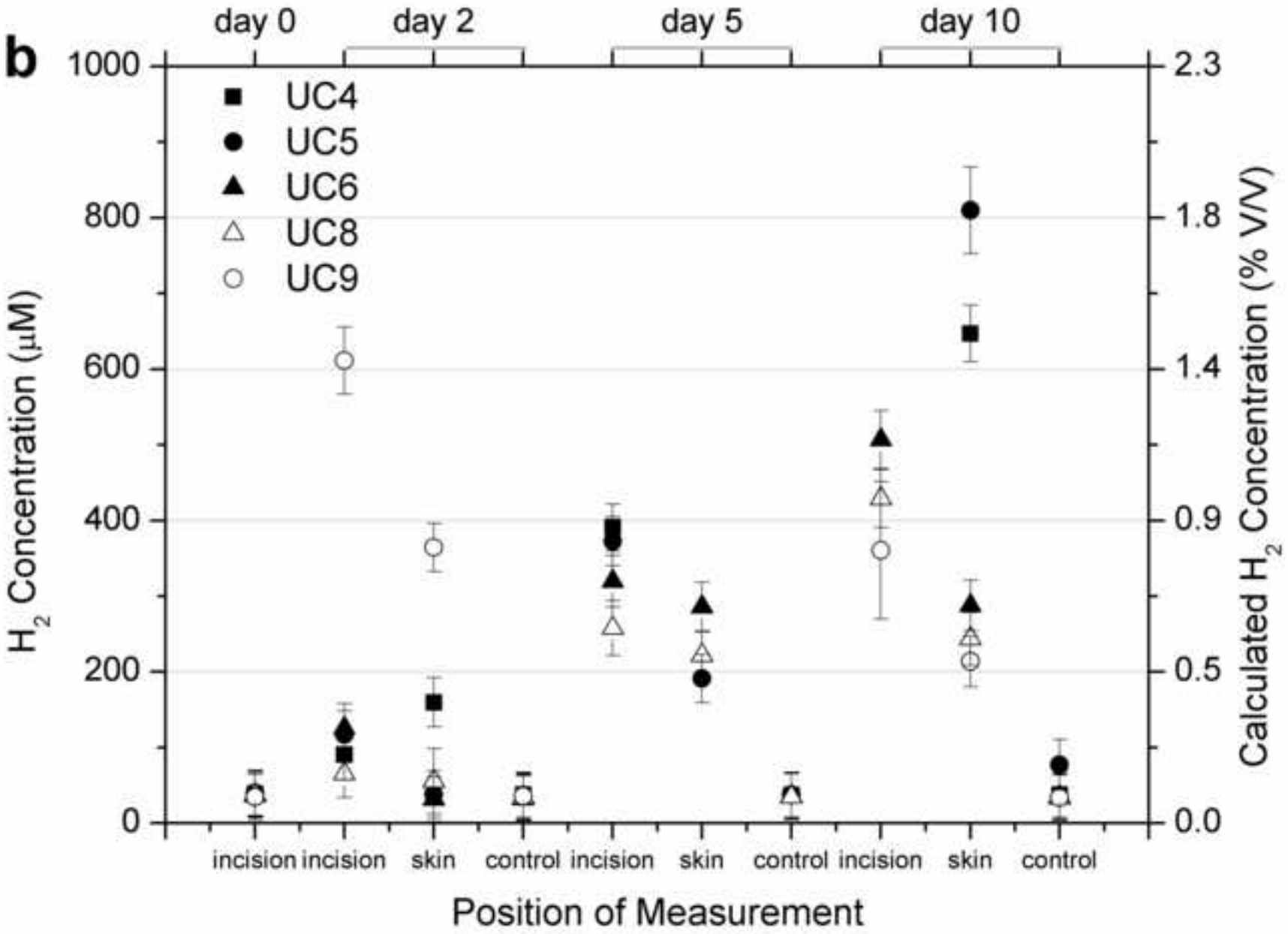

Figure 4a

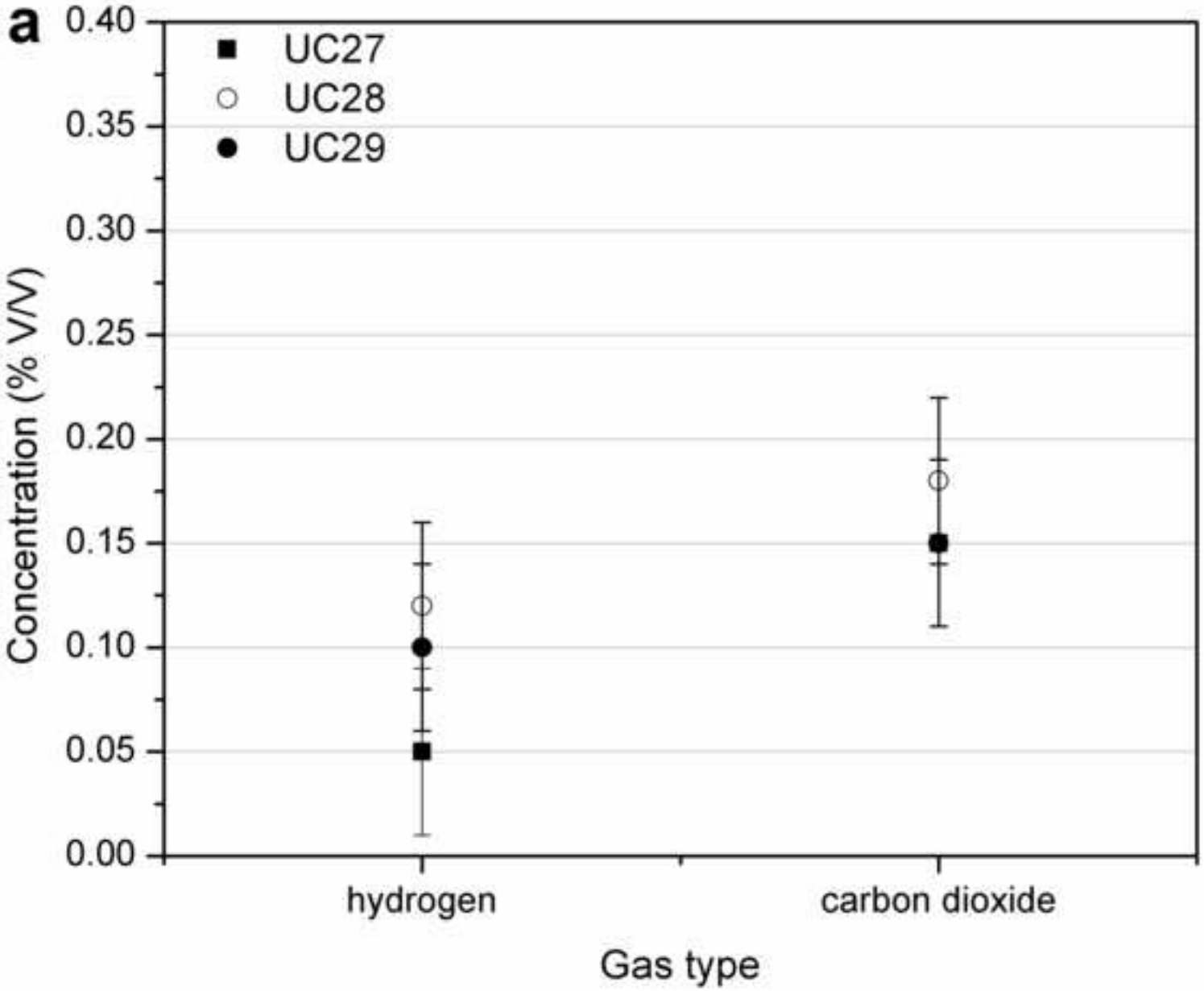

Figure 4b

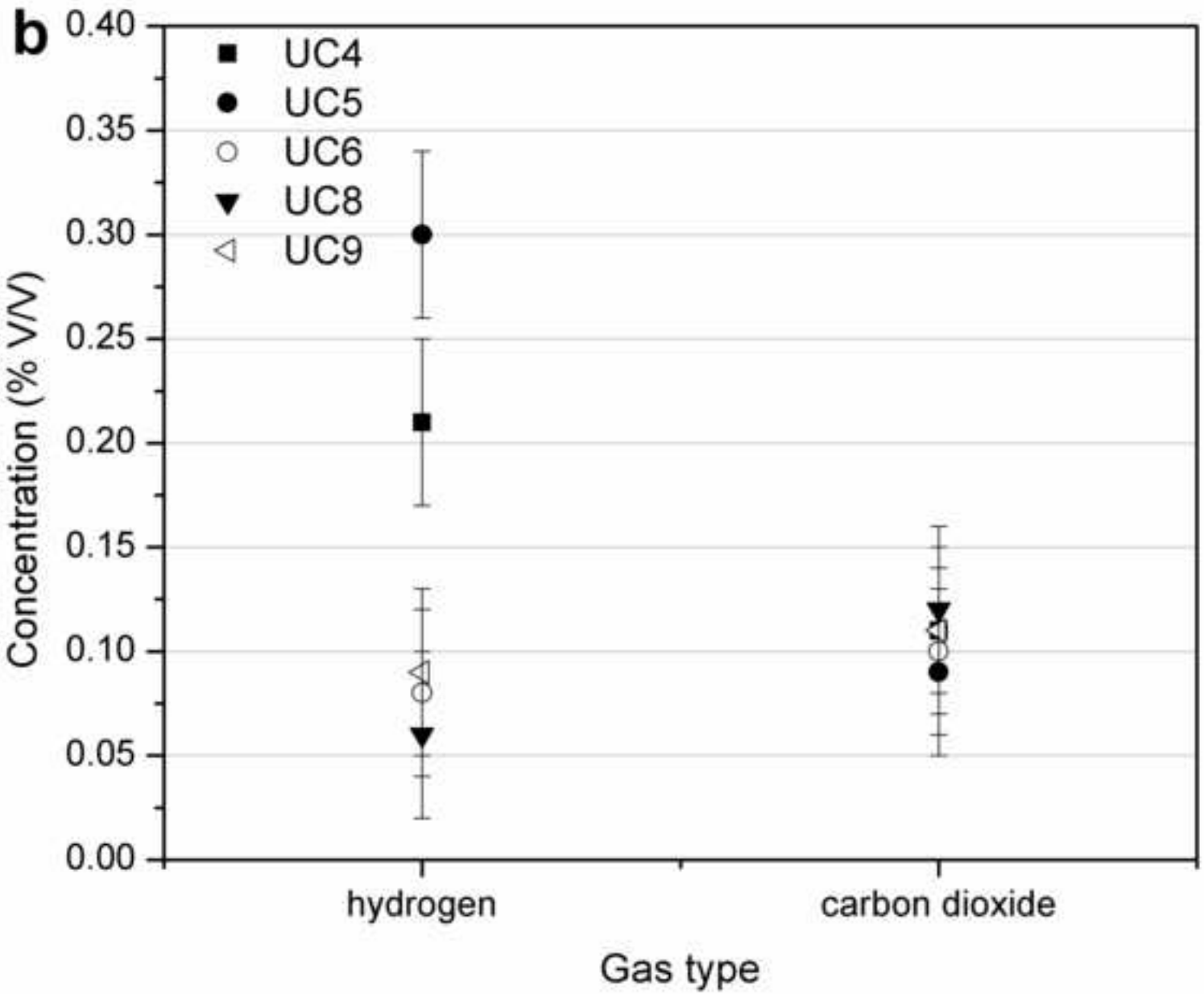

Figure 5

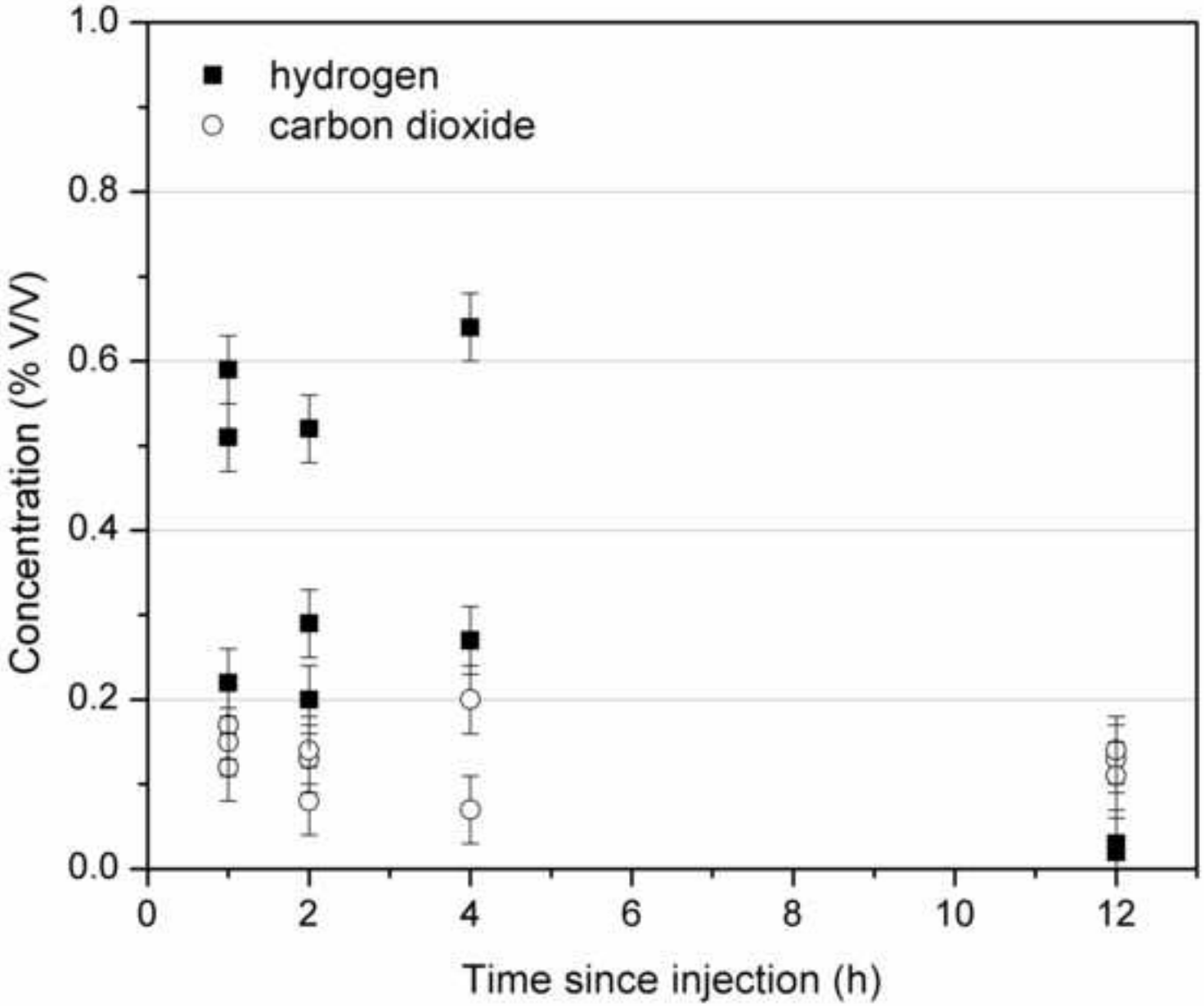

Figure 6A

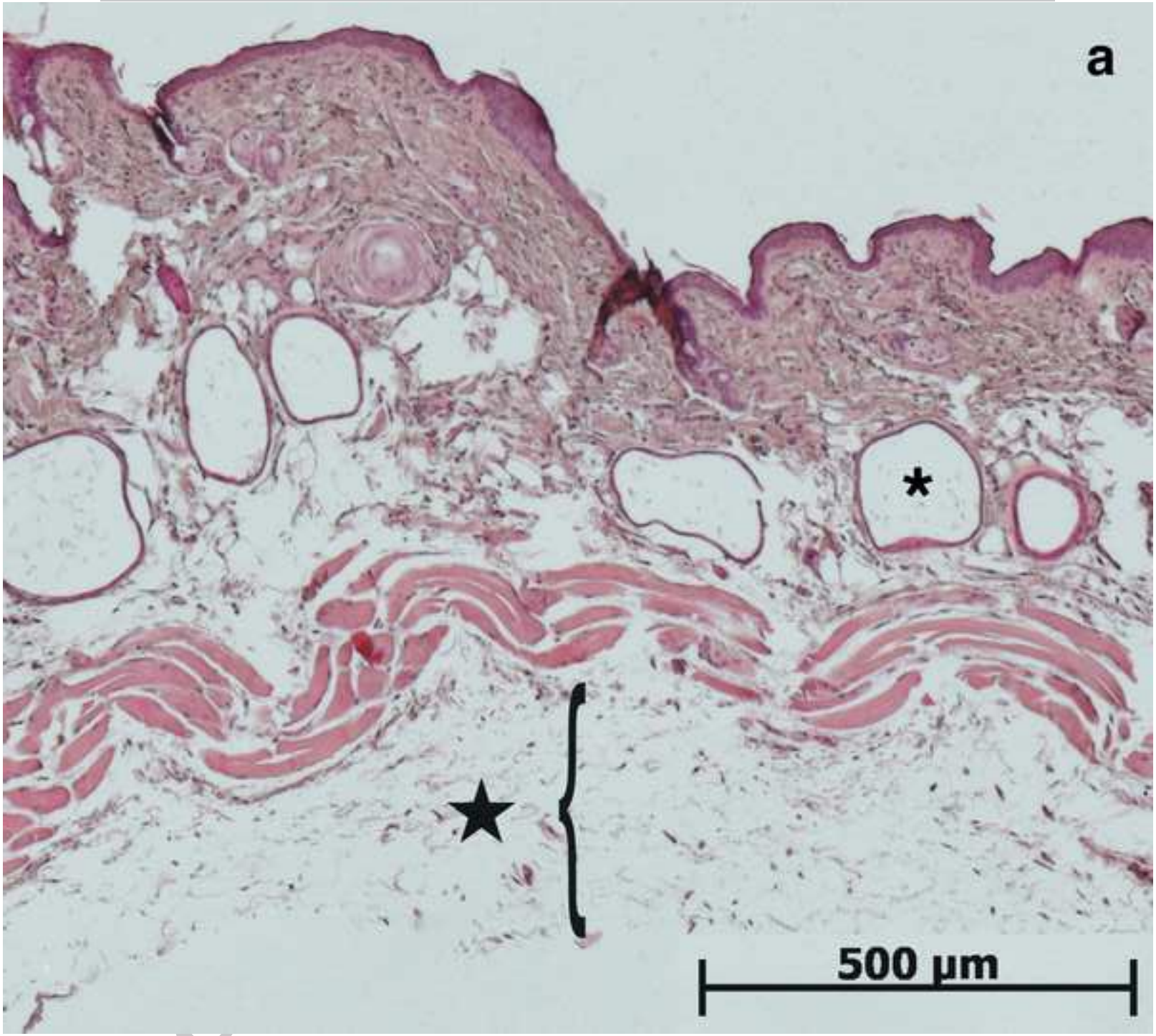

Figure 6B

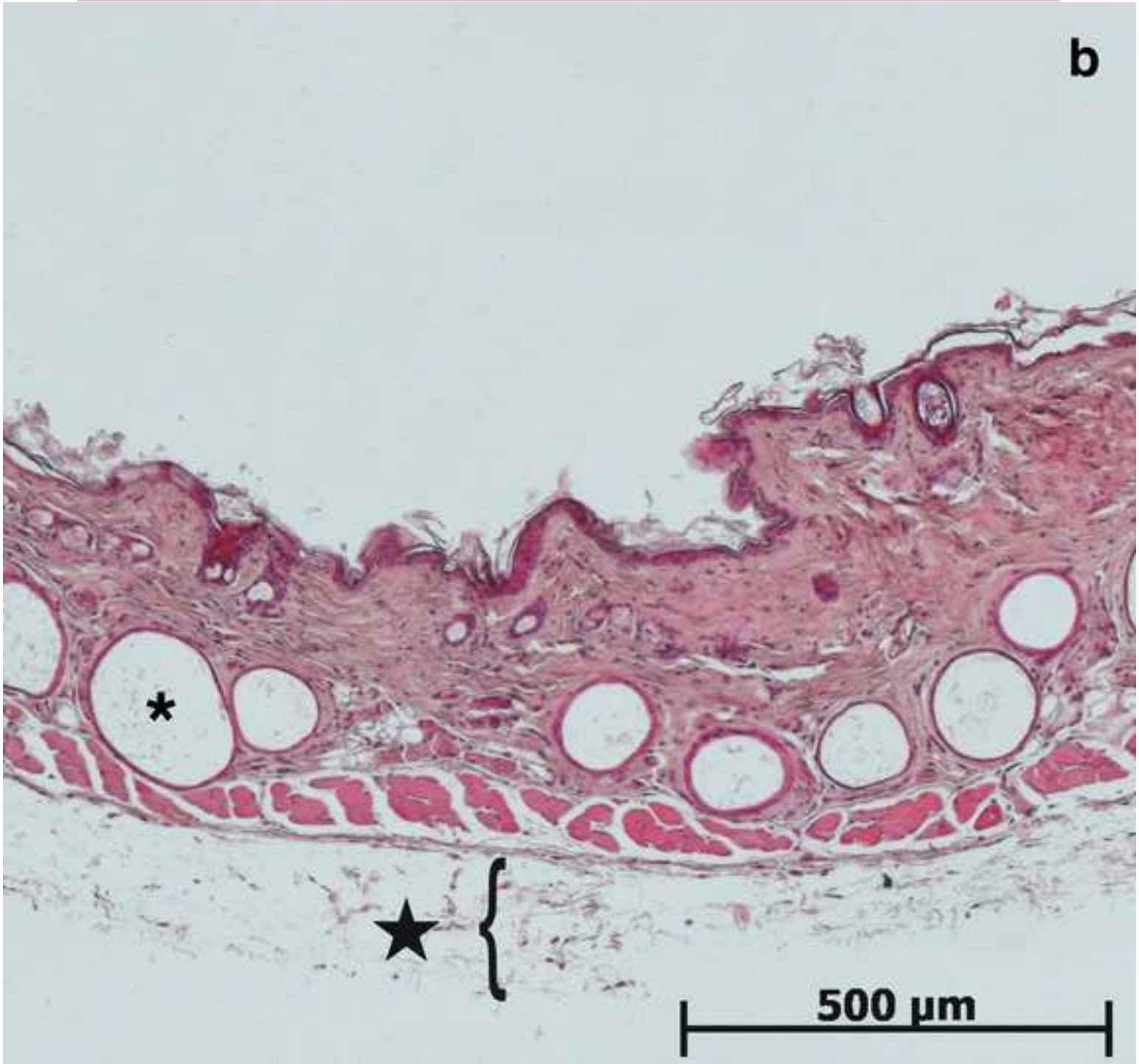

Figure 6C

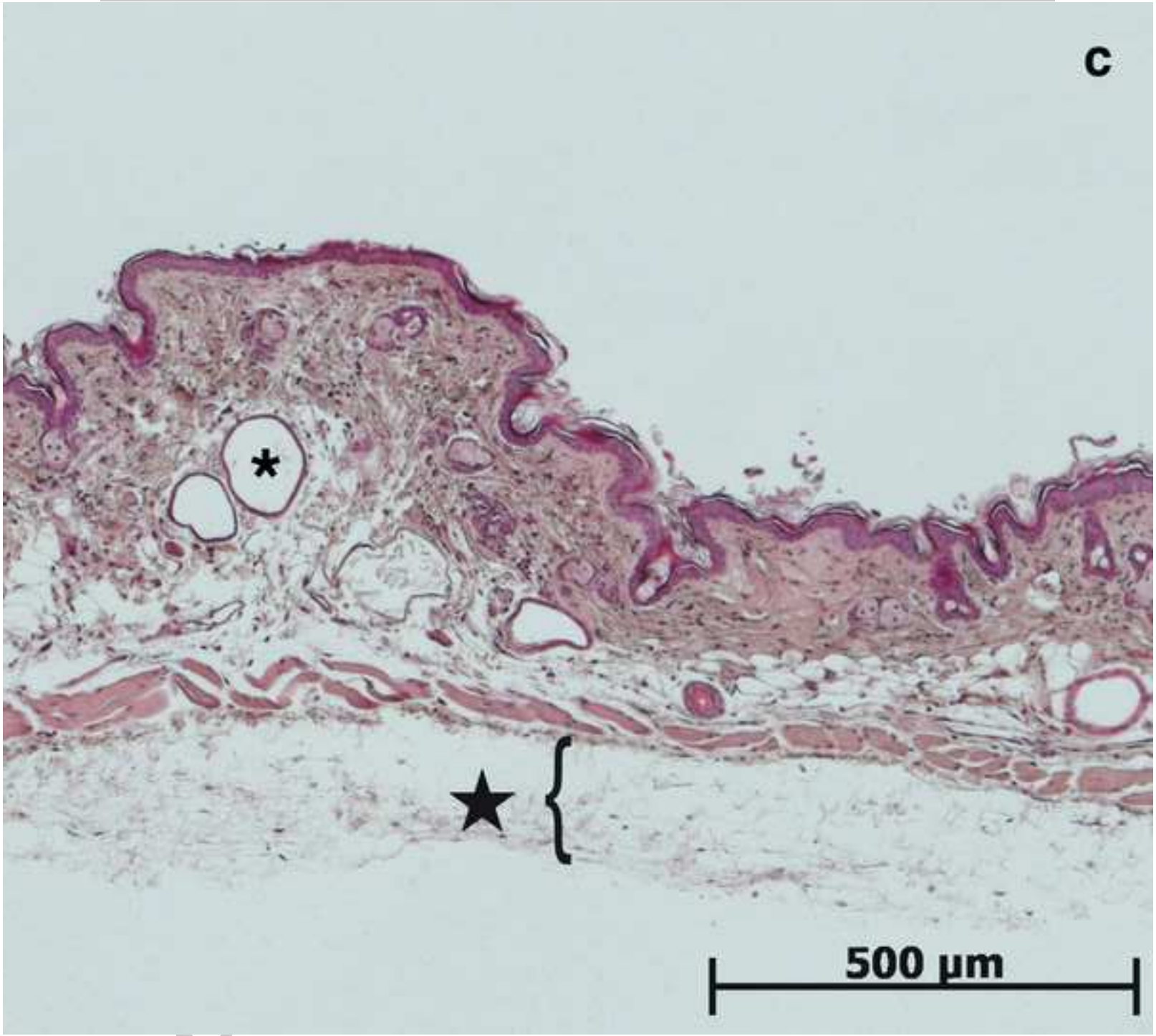

Figure 7

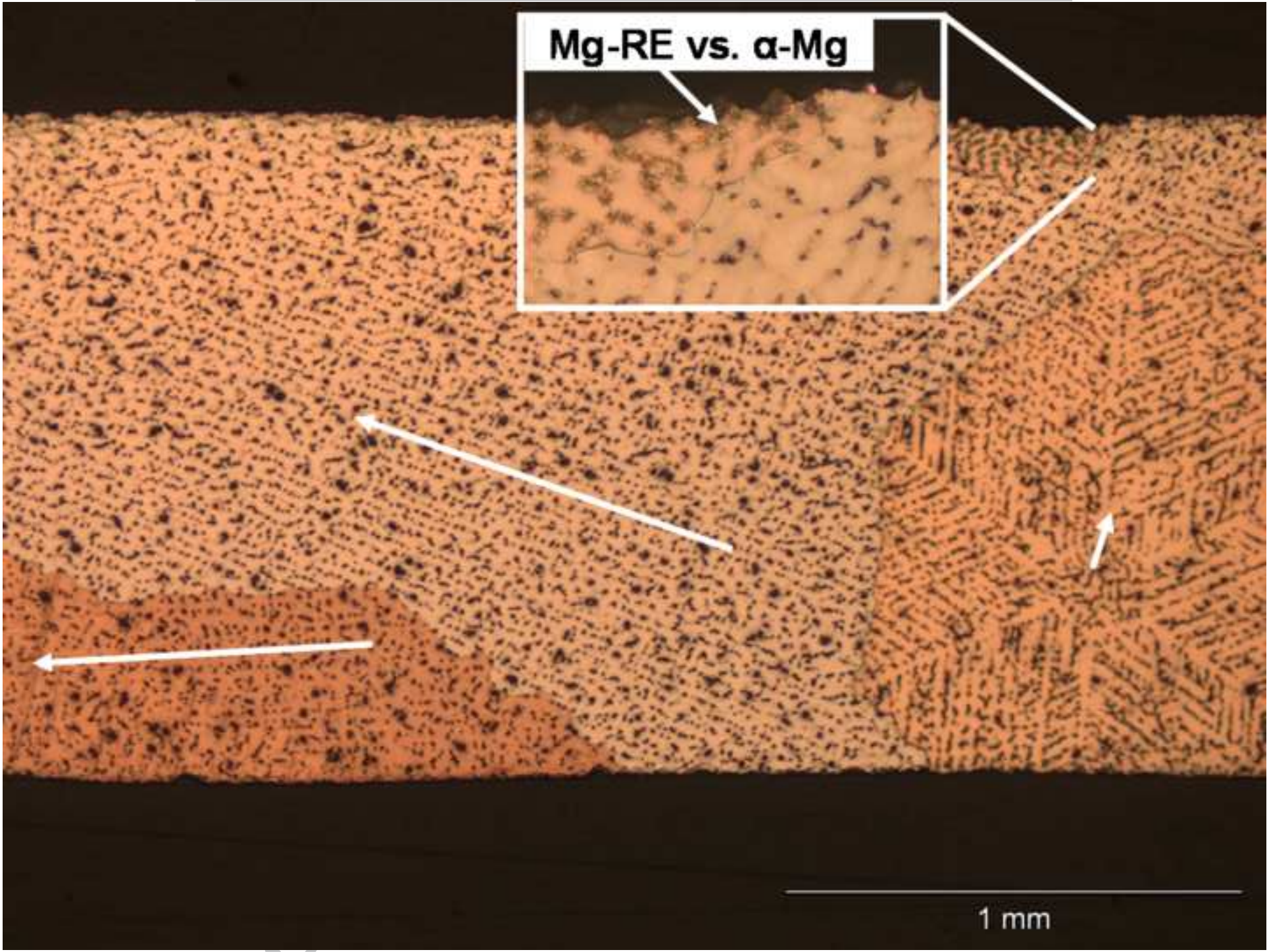

Figure 8